Energy & Environmental Science

PAPER

View Article Online
View Journal | View Issue

Cite this: *Energy Environ. Sci.*, 2016, **9**, 1095

"Wiring" redox-active polyoxometalates to carbon nanotubes using a sonication-driven periodic functionalization strategy†

Jun Hu,[a] Yuanchun Ji,[ab] Wei Chen,[a] Carsten Streb*[b] and Yu-Fei Song*[a]

Received 8th October 2015,
Accepted 13th January 2016

DOI: 10.1039/c5ee03084f

www.rsc.org/ees

The periodic deposition of redox-active polyoxometalate(POM) nanocrystals on single-walled carbon nanotubes (CNTs) using ultrasonication is reported. The new method allows the controlled formation of 1D POM/CNT nanocomposites where crystals of redox-active POMs of tunable size and shape are deposited at regular intervals on the CNTs. The nanostructure and chemical features of the composite can be tuned through the ultrasonication intensity and time as well as the chemical make-up of the polyoxometalates and their counter-cations. The materials obtained show excellent electrochemical performance as anode materials in lithium-ion- batteries (LIBs) featuring discharge capacities of 850 mA h g^{-1} for up to 100 cycles.The modular nano-fabrication approach can open new avenues for the bottom-up"wiring" of functional molecular materials to electrically conductive substrates.

Broader context

Modern battery electrodes rely on the intimate electrical contacting between electron storage and electron transport sites. Often, the bulk electrical conductivity of promising battery electrodes is rather low, so that electrical contacting with conductive substrates on the nanoscale is required. Mechanical stress during battery charging and discharging can cause loss of contact between conductive substrate and the electron storage components, ultimately leading to battery failure. Here, a novel nanostructuring approach is presented where highly redox-active molecular metal oxides, so-called polyoxometalates (POMs) are deposited on conductive carbon nanotubes (CNTs) to give high-performance lithium-ion battery electrodes. The periodic deposition of the POMs along the single-walled CNTs is achieved using an ultrasonication patterning approach which allows control over the precise nanostructure of the composite material. It is shown that the fabrication procedure gives access to highly stable lithium-ion battery electrodes with superior electrochemical performance allowing the use of a wide range of POMs.

Introduction

One-dimensional (1D) carbon nanotubes (CNTs) have attracted worldwide attention owing to their superior optical, electrical and mechanical properties.[1–4] Typically, CNTs are obtained as insoluble bundles due to inter-CNT π–π and van der Waals interactions. The actual capacity of CNTs is much less than the theoretical value is because of the strong π–π stacking of the tubes, leading to an inner space capacity decrease with the bunch tubes. To allow solution-processing of CNTs, breaking up the CNT bundles is critical. However, non-functionalized CNTs are insoluble in typical organic solvents; thus, CNTs functionalization by chemical means has been introduced to improve the solubility, solution compatibility and chemical functionality of CNTs.[5–8] Two main functionalization pathways can be distinguished. Covalent CNT functionalization allows the controlled attachment of functional pendant groups to the CNTs framework, giving chemically and mechanically stable materials. However, as CNTs functionalization requires the conversion of planar sp^2-hybridized carbon atoms into strained tetrahedral sp^3-hybridized atoms, this approach often results in the disruption of the CNTs conjugation, leading to reduced electrical and mechanical performance of the CNTs.[8,9] In contrast, non-covalent CNTs functionalization uses supramolecular interactions (π–π-interactions, van der Waals interactions, *etc.*) to reversibly link surface-active species such as surfactants, oligomers, biomolecules and polymers to CNTs.[10–13] This approach does not affect the structural and electronic integrity of the CNTs. However, due to the relatively weaker binding interactions, the attachment of the surface groups to the CNTs is not as chemically and mechanically robust as covalently attached groups.[8]

[a] *State Key Laboratory of Chemical Resource Engineering, Beijing University of Chemical Technology, 100029 Beijing, P. R. China. E-mail: songyufei@hotmail.com, songyf@mail.buct.edu.cn; Fax: +86 10-64411832; Tel: +86 10-64411832*

[b] *Institute of Inorganic Chemistry I, Ulm University, Albert-Einstein-Allee 11, 89081 Ulm, Germany. E-mail: carsten.streb@uni-ulm.de*

† Electronic supplementary information (ESI) available. See DOI: 10.1039/c5ee03084f

In recent years, the periodic functionalization of CNTs has become a highly attractive field of research as it provides a unique opportunity to nano-pattern CNTs, giving well-ordered, functional structures for optical and electronic applications.[14] Periodic functionalization of CNTs is still extremely challenging as one needs to control surface attachment of functional groups on the nanometre level. Consequently, only few methods have thus far been established to reliably introduce periodic functional features on CNTs. Worsley *et al.* showed that long-range, regular patterns of functional organic surface groups can be introduced when covalently functionalizing CNTs using the Bingel reaction.[15] In a pioneering study, Li *et al.* reported the non-covalent periodic patterning of polymers on individual CNTs using a crystallization-driven approach, giving lamellar nanostructures with tuneable size and spacing of the lamellae. This work has inspired us as it illustrates the ability to controllably introduce functional species on CNTs in the nanometre domain.[16]

In this study, we present the CNTs which are periodically patterned with redox-active polyoxometalates (POMs) to give novel high-performance battery components. POMs are anionic metal oxides of V, Mo, W, *etc.* with unmatched physico-chemical properties (redox-, electro- and photoactivity, *etc.*) and a rich structural chemistry.[17–29] The field of POM/CNT nanocomposites has recently seen tremendous growth as the composites boast highly desirable properties for energy conversion and storage.[6,7] Currently, the electrical "wiring" of POMs to CNTs is still a major challenge and facile bulk methods are required to tune the overall electric performance of POM/CNT nanocomposites.

Several approaches have recently been developed, including surface functionalization of CNTs with organic cations which then allow the electrostatic binding of POM anions.[30] However, this approach often gives materials with reduced structural stability, thus limiting their practical application. We have recently shown that organo-functionalized POMs featuring extended aromatic groups (*e.g.* pyrene) can be used to non-covalently link these species to the surface of CNTs through π–π interactions.[8] Also, covalent CNT functionalization with POMs has been achieved through the reaction of acyl chloride-functionalized CNTs with organo-amine functionalized POMs, leading to the formation of covalent amide bonds.[6,7] Importantly, the covalently linked POM/CNT feature significantly better electrochemical performance compared with the purely electrostatically linked composites.[7] However, as only a limited number of POM anions can be organically functionalized, the covalent attachment of POMs to CNTs is critically limited.[31] Further, the covalent linkage procedure can introduce surface defects in the CNTs leading to reduced performance in energy conversion and storage. Thus, facile and universal synthetic routes are required which allow the stable linkage of POMs to CNTs while retaining the structural and electronic integrity of the CNTs.

Inspired by previous work,[14–16,32,33] we herein report the use of sonochemistry for the crystallization-driven nanopatterning of POMs on single-walled CNTs leading to functionally and structurally stable POM/CNT nanocomposites. The POM crystal size and morphology can be tuned by controlling the ultrasonication parameters. The procedure is applicable to a wide range of POMs, allowing the tuning of critical materials properties over a wide range. Here, the excellent performance of POM/CNT nanocomposites as anode materials in lithium ion batteries (LIBs) is reported.

Experimental section

Materials

All reagents were obtained from Alfa Aesar Company and used as received unless stated otherwise. Single-walled carbon nanotubes (CNTs, purity >95%) were purchased from Chengdu Organic Chemicals Co. Ltd, Chinese Science Academy.

Measurements

FT-IR spectroscopy was measured using KBr pellets and recorded on a NICOLET 6700 instrument. Scanning electron microscopy (SEM) images was obtained using a Zeiss Supra 55 SEM. Transmission electron microscopy (TEM) micrographs were recorded using a Hitachi H-800 instrument. HRTEM images were conducted on a JEOL JEM-2010 electron microscope operating at 200 kV. Raman spectra were measured on a Renishaw Raman spectrometer at a laser excitation wavelength of 633 nm. Thermogravimetric (TG) analysis was done on STA-449C Jupiter (HCT-2 Corporation, China) with a heating rate of 10 °C min^{-1} from 25 to 1000 °C in flowing N_2. N_2 adsorption–desorption isotherms were measured using a Quantachrome Autosorb-1 system at liquid nitrogen temperature. X-ray photoelectron spectroscopy (XPS) measurements were performed using monochromatized Al Kα radiation (PHI Quantera SXM). Cyclic Voltammetry (CV) and electrochemical impedance spectroscopy (EIS) were carried out on a CHI660E electrochemical workstation. Battery capacity and galvanostatic charging/discharging were measured on a LAND-CT2001A battery test system within a voltage range of 0–3.0 V.

Polyoxometalates (POMs) preparation

The POM salts employed in this study were prepared as shown in Table 1.

Preparation of the POM/CNT nanocomposites

10 mg of purified single-walled CNTs were dispersed in 10 mL of methanol under 60 kHz ultrasonication for 1 h at room temperature. Then, 20 mg of the respective POM salt in 1 mL acetonitrile was added to the CNTs dispersion and the dispersion was sonicated at the corresponding frequency for the desired amount of time. The composite was isolated by centrifugation and washed three times with dry methanol. The nanocomposites were dried in a vacuum oven at 40 °C overnight.

Preparation of lithium-ion batteries anode material

TBA-$PMo_{11}V$ was used as a prototype POM. The as-prepared TBA-$PMo_{11}V$/CNTs nanocomposites were used as anode material for rechargeable lithium-ion batteries. Electrochemical measurements were carried out using coin-type cells. The electrodes were prepared by mixing TBA-$PMo_{11}V$/CNTs, carbon black, and poly(vinylidene fluoride) (PVDF) at a weight ratio of 80 : 10 : 10;

Table 1 POM salts employed in this study

Entry no	POM-salt	Abbreviation	Ref.
1	$H_3[PMo_{12}O_{40}]\cdot nH_2O$	PMo_{12}	34
2	$H_3[PW_{12}O_{40}]\cdot nH_2O$	PW_{12}	34
3	$H_3[SiW_{12}O_{40}]\cdot nH_2O$	SiW_{12}	34
4	$H_4[PMo_{11}VO_{40}]\cdot 13H_2O$	$PMo_{11}V$	34
5	$H_5[PMo_{10}V_2O_{40}]\cdot 9H_2O$	$PMo_{10}V_2$	34
6	$H_6[PMo_9V_3O_{40}]\cdot 12H_2O$	PMo_9V_3	34
7	$H_4[PW_{11}VO_{40}]\cdot 10H_2O$	$PW_{11}V$	34
8	$TBA_3[PMo_{12}O_{40}]$[a]	TBA-PMo_{12}	35
9	$TBA_3[PW_{12}O_{40}]$	TBA-PW_{12}	35[b]
10	$TBA_3[SiW_{12}O_{40}]$	TBA-SiW_{12}	35[b]
11	$TBA_4[PMo_{11}VO_{40}]$	TBA-$PMo_{11}V$	35[b]
12	$TBA_5[PMo_{10}V_2O_{40}]$	TBA-$PMo_{10}V_2$	35[b]
13	$TBA_6[PMo_9V_3O_{40}]$	TBA-PMo_9V_3	35[b]
14	$TBA_4[PW_{11}VO_{40}]$	TBA-$PW_{11}V$	35[b]
15	$TOA_4[PMo_{11}VO_{40}]$[c]	TOA-$PMo_{11}V$	36
16	$DDA_4[PMo_{11}VO_{40}]$[d]	DDA-$PMo_{11}V$	36
17	$STA_4[PMo_{11}VO_{40}]$[e]	STA-$PMo_{11}V$	36

[a] TBA: tetra-*n*-butylammonium. [b] The syntheses were carried out as described in ref. 35 using the respective POM anion shown in Table 1. [c] TOA: tetra-*n*-octylammonium. [d] DDA: dodecyltrimethylammonium. [e] STA: steartrimonium.

this was pasted on a Cu foil[37] (the mass loading of the active materials on the current collector is about 2.64 mg, and the total weight is 3.31 mg). The electrode was dried under vacuum. The coin cells were assembled in an argon-filled glove box with the anode as-fabricated, metallic lithium foil as a counter electrode, and a 1 M $LiPF_6$ solution in ethylene carbonate (EC)/diethyl carbonate (DEC) (1 : 1 v : v) as electrolyte. The specific charge/discharge capacities were calculated based on the POM/CNT nanocomposites material.

Results and discussion

Scheme 1 shows the crystallization-driven periodic functionalization of CNTs with POM nanocrystals: initial CNTs dispersion in methanol is achieved by ultrasonication of the CNT bundles to interrupt the CNT bundle packing.[38] When POM salts (here: TBA (tetra-*n*-butylammonium) salts of Keggin-type POMs, see Table 1) are added to the CNTs dispersion, electrostatic interactions between the CNTs surface, TBA cations and POM anions are established, resulting in the adsorption of the POMs onto the CNTs.[30] When this process is performed under sustained low-intensity, high frequency ultrasound (>50 kHz),[39] we observe that the POM deposition can be spatially controlled in the nanometer regime.

To investigate the effects of sonication-driven POM deposition on CNTs, we initially explored the consequences of varying ultrasonic power intensity on the crystallization of the model POM $TBA_4[PMo_{11}VO_{40}]$ (=TBA-$PMo_{11}V$) on CNTs. To this end, the synthetic procedure outlined above (Experimental section) was used to form POM/CNT nanocomposites which were investigated using scanning electron microscopy (SEM). Notably, when the procedure was performed without sonication, no de-bundling of the CNTs and no deposition of POM crystals on CNTs was observed (Fig. 1).

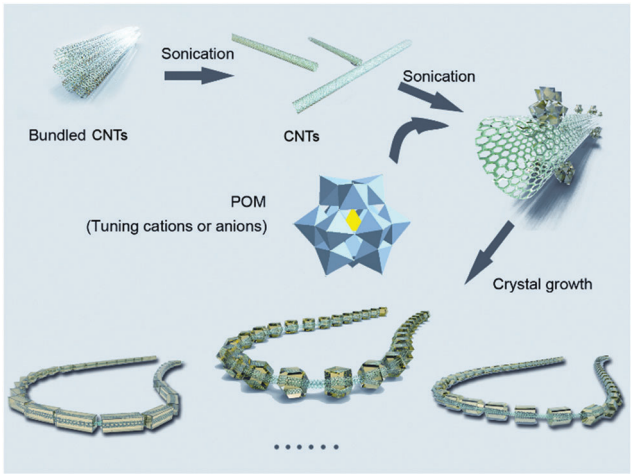

Scheme 1 Schematic illustration of the ultrasonication-driven periodic patterning of POM nanocrystals on CNTs.

At intensities of 0.34 W cm^{-2}, periodic deposition of POM crystals (diameter ~20 nm) on the surface of CNTs is observed. Notably, the crystals are not loosely attached to the CNTs but the CNTs passes through the POM crystals. When the ultrasonication intensity is increased to 0.50–0.83 W cm^{-2} under otherwise identical conditions (and reaction times), the POM crystal size reproducibly increases to ~200 nm and a rhombic dodecahedral POM crystal morphology with rounded edges is observed. The results show that ultrasonication can be used to direct the size and morphology of crystalline POM nanostructures deposited on CNTs.

The effects of ultrasonication time on the POM crystal deposition on CNTs at sonication intensity of 0.83 W cm^{-2} and sonication frequency of 60 kHz was explored next. Variation of the sonication time between 1–48 h showed significant changes of the POM crystal morphology. For short sonication times (t = 1–3 h), the POM crystals feature irregular polyhedral shapes; also, over this period they grow in size from 20 nm to 50 nm (t = 2–3 h). After t = 4 h, regular rhombic dodecahedron crystals with diameters of ~200 nm are observed. When the sonication time is increased further, crystal growth is mainly observed along one axis, giving elongated hexagons with

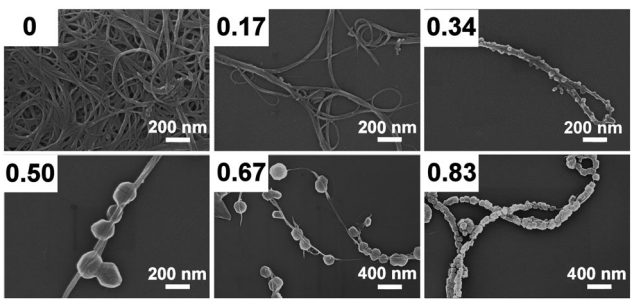

Fig. 1 POM/CNT nanocomposites formation: variation of ultrasonic power intensity (inset numbers, unit: W cm^{-2}) gives control over the POM-crystal size and morphology. Sonication time = 4 h, sonication frequency = 60 kHz.

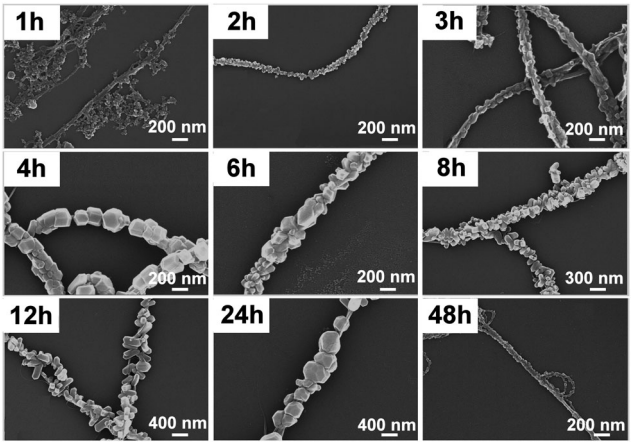

Fig. 2 The influence of sonication time on the crystallization of TBA-$PMo_{11}V$ on CNTs. Sonication intensity = 0.83 W cm^{-2}, sonication frequency = 60 kHz.

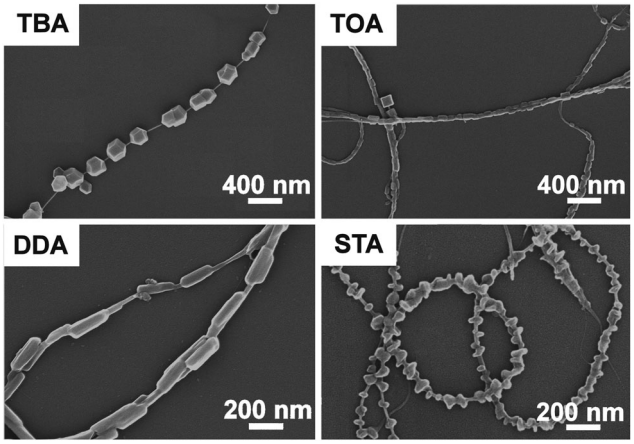

Fig. 3 Effect of various cations on the deposition of $PMo_{11}V$ on CNTs. TBA: tetra-*n*-butylammonium; TOA: tetra-*n*-octylammonium; DDA: dodecyltrimethyl-ammonium; STA: steartrimonium. Sonication intensity = 0.83 W cm^{-2}, sonication time = 4 h; sonication frequency = 60 kHz.

dimensions of approx. 200 × 500 nm ($W \times L$) after t = 12 h. After t = 24 h, the crystals grow to an overall size of approx. 400 nm and adopt a more spherical shape. After t = 48 h, the well-ordered arrangement of the POM crystals is no longer observed, suggesting that "over"-sonication destroys the POM nanostructures. In summary, this analysis shows that sonication time can be used to control the size and morphology of the POM-crystals deposited (Fig. 2).

In the following study, the general adaptability of the synthetic method was investigated by varying the type of cations present whilst using identical POM anions ($PMo_{11}V$) as prototypes: tetra-*n*-octylammonium salts (TOA-$PMo_{11}V$), dodecyltrimethyl-ammonium salts (DDA-$PMo_{11}V$) and steartrimonium salts (STA-$PMo_{11}V$) were used as representative organo-cations. As shown in Fig. 3, cation variation resulted in a change of morphology of the POM-crystals deposited on the CNTs. For example, the TBA-$PMo_{11}V$/CNTs nanocomposites show chain-like rhombic dodecahedral crystals (diameter ~200 nm), whereas the TOA-$PMo_{11}V$/CNT nanocomposites feature cuboid POM crystals (~100 nm). For the DDA-$PMo_{11}V$/CNTs composites, rod-like POM-crystals (length ~250 nm) wrapped around the CNTs are observed. For STA-$PMo_{11}V$/CNTs composites, rod-like crystals (~100 nm) are observed where the elongated axis grows perpendicular to the CNTs. This study highlights that cations can be used to control size, shape and growth orientation of the POM crystals on the CNTs.

In the next study, the type of POM anion was varied whilst keeping the cation TBA unchanged. This is a particularly important aspect, as POM variation allows the modification of the chemical and electronic properties of the crystals. A selection of Keggin-based molybdate and tungstate clusters (see Table 1, entries 8–14) were employed to highlight the general applicability. For the POM anions studied, two main crystal morphologies are observed (see Fig. 4). When TBA-PMo_9V_3, TBA-$PMo_{10}V_2$, TBA-PMo_{12} or TBA-PW_{12} are employed, rhombic dodecahedron-shaped crystals of varying size are periodically arranged along the CNTs. In contrast, when TBA-$PW_{11}V$ or TBA-SiW_{12} are used, rod-like crystal growth perpendicular to the CNTs is observed. The results highlight that a variety of Keggin-based POMs with diverse redox-chemistry can be deposited on CNTs. Further, the type of anion affects the crystal morphology observed.

Our previous results demonstrated that surface functionalization of CNTs with POMs can introduce desirable electronic properties and enhance the CNTs processability.[6–8] These combined features have led to significant interest for the design of POM/CNT electrode materials for lithium-ion batteries (LIB).[30,38,40,41]

Based on the promising features of the periodically functionalized POM/CNT nanocomposites reported here, initial electrochemical studies of the nanocomposites as LIB electrodes were performed.[41] As a model system, the TBA-$PMo_{11}V$/CNT nanocomposites with regular rhombic dodecahedron morphology (Fig. 3, TBA-$PMo_{11}V$/CNTs, sonication intensity 0.83 W cm^{-2}, sonication frequency 60 kHz sonication time 4 h) were used and incorporated in a standard coin-cell LIB (see Experimental section and ESI†). The material was chosen due the underlying redox-chemistry of the $PMo_{11}V$ cluster as well as the thermal stability (see Fig. S2, ESI†) and the high specific surface area of approx. 140 $m^2\ g^{-1}$ (Fig. S3, ESI†).

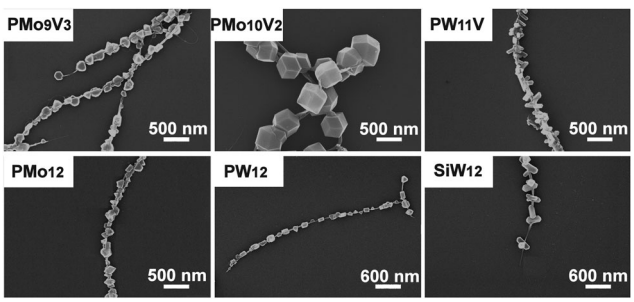

Fig. 4 Effect of POM anion variation (cation: TBA) on the POM/CNT morphology. Sonication intensity = 0.83 W cm^{-2}, sonication time = 4 h; sonication frequency = 60 kHz.

Fig. 5a shows the first and second charge–discharge cycle of the TBA-$PMo_{11}V$/CNTs electrode at a current density of 0.5 mA cm^{-2}. The first discharge capacity of is 3014.1 mA h g^{-1}; in the second cycle, the discharge capacity decreases to 1052.6 mA h g^{-1}. This behaviour is well known and is associated with the formation of a solid–electrolyte interface[42] (see below) Over subsequent cycles, the specific capacity stabilized at *ca.* 850 mA h g^{-1} (Table 2 and Fig. 5). The high specific capacity of the POM/CNT composites illustrates the efficient electrical "wiring" between both components. This is further verified when comparing the nanocomposite performance with the pure components and the physical mixture of the components. As shown in Table 2, significantly higher specific capacities are found for the nanocomposite compared with the reference systems, highlighting the optimized electrochemical performance of the "wired" system. The studies were carried out under identical conditions.

Fig. 5b displays the cycling stability and capacity retention of the TBA-$PMo_{11}V$/CNTs electrode at a current density of 0.5 mA cm^{-2}: after an initial drop, the capacity remains stable at *ca.* 850 mA h g^{-1} for 100 cycles. The electrochemical performance and stability of the present system is significantly higher compared with related systems (see Table 2 and Table S1, ESI†). Electrode reversibility was examined to evaluate the technological importance of the composites: the initial coulombic efficiency of the TBA-$PMo_{11}V$/CNTs nanocomposites is only 34.9%; after 20 cycles, the value reaches a plateau at ~99% where it remains stable, thus demonstrating excellent cycling stability of the composite.

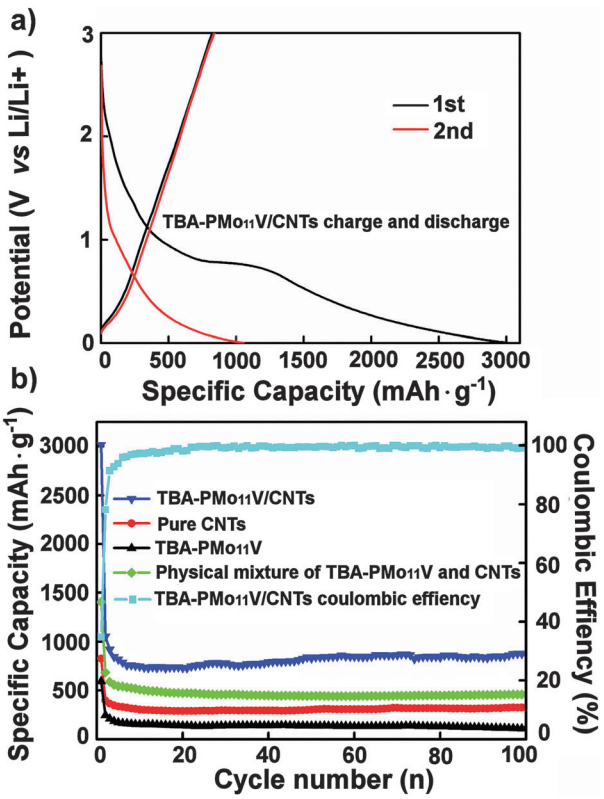

Fig. 5 (a) The first and second charging and discharging cycle of the LIB prototype based on the TBA-$PMo_{11}V$/CNTs composite; (b) the discharge capacity of the nanocomposite (blue), pure CNTs (red), pure POM (black) and the physical mixture (non-wired) of POM and CNTs (green) as well as the coulombic efficiency of the nanocomposite (light blue), current density is 0.5 mA cm^{-2}.

Table 2 Performance of LIB anodes based on the new nanocomposites, the pure components and the physical mixture of the components[a]

Electrode type	Current density/mA cm^{-2}	Specific capacity[b]/mA h g^{-1}
TBA-$PMo_{11}V$/CNTs nanocomposites	0.5	850
Pure CNTs	0.5	324
Pure TBA-$PMo_{11}V$	0.5	107
Physical mixture	0.5	460

[a] Electrodes were prepared based on identical mass-content of the respective component(s). [b] Determined after 100 cycles.

Rate performance and cycling stability during the lithium ion insertion/extraction are key factors for practical battery applications. Here, we expected the nanocomposites to show superior lithium ion diffusion due to their high specific surface area (see above and Fig. S3, ESI†). To this end, the rate performance of the TBA-$PMo_{11}V$/CNTs nanocomposites was evaluated at current densities between 0.05 and 1 mA cm^{-2} using a cut-off voltage between 0 and 3.0 V *vs.* Li/Li^+ (Fig. 6a). As expected, higher current densities result in lower discharge capacities. For example, the discharge capacity at 0.05 mA cm^{-2} is 1531.7 mA h g^{-1} and it decreases to 565 mA h g^{-1} at a current density of 1 mA cm^{-2}. When the current density is re-set to the original value after 70 cycles, the original discharge capacity is recovered, indicating the high structural stability of the TBA-$PMo_{11}V$/CNTs composites. Furthermore, the stable cycle performance at higher rates indicates fast solid-state Li^+ ion diffusion and is indicative of a short diffusion path length and structural stability.[7]

Cyclic voltammetry of the TBA-$PMo_{11}V$/CNTs nanocomposites (Fig. 6b, scan rate: 0.1 mV s^{-1}; scan range: 0–3 V *vs.* Li/Li^+) shows an irreversible reduction peak at approx. 0.7 V in the first reduction run, which indicates the formation of a solid electrolyte interphase (SEI).[42] However, this peak disappears in the subsequent cycles. The reduction signal between 0.0–0.2 V can be attributed to the Li^+ insertion reaction. The corresponding oxidation peak at *ca.* 0.2 V observed in the charging process is assigned to Li^+ extraction from the TBA-$PMo_{11}V$/CNTs nanocomposites. This signal can be observed in the subsequent cycles, suggesting that Li^+ insertion/extraction is reversible in the TBA-$PMo_{11}V$/CNTs nanocomposites under the given experimental conditions. In summary, the electrochemical studies of the periodically patterned POM/CNT nanocomposites highlight the effective electrical "wiring" of the POM crystals to the CNTs. As a consequence, significantly enhanced discharge capacities compared with pure CNTs and pure POMs are found[42,43] (see also Table S1, ESI†).

In order to confirm the enhancement of electrochemical activity of the TBA-$PMo_{11}V$/CNTs as anode material, AC electrochemical impedance spectroscopy has been carried out to obtain insight into the electrochemical behaviour of the corresponding materials.

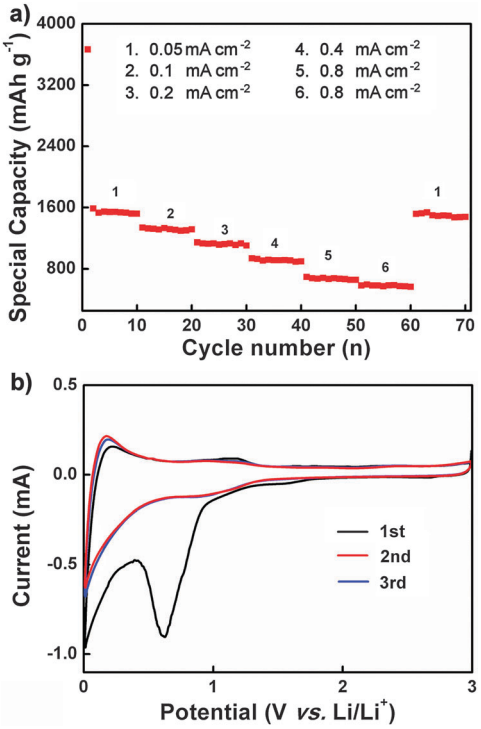

Fig. 6 (a) Rate performance of the TBA-$PMo_{11}V$/CNTs nanocomposites electrode at current densities of 0.05 to 1 mA cm^{-2}, (b) cyclic voltammograms of TBA-$PMo_{11}V$/CNTs with a scan rate of 0.1 mV s^{-1} at the potential range of 0–3 V.

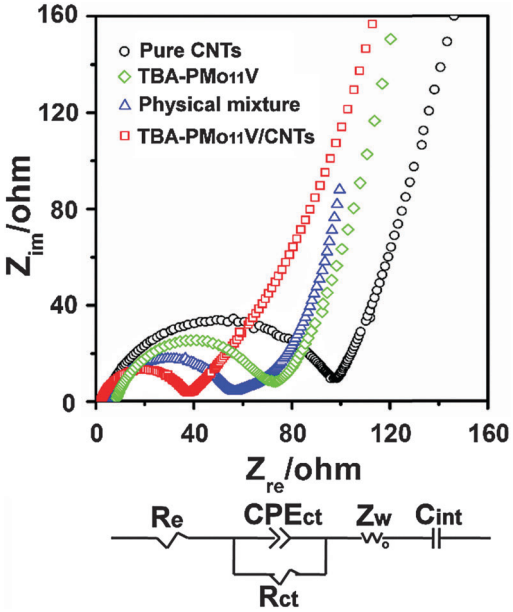

Fig. 7 Nyquist plots of TBA-$PMo_{11}V$/CNTs, the physical mixture of TBA-$PMo_{11}V$ and CNTs, TBA-$PMo_{11}V$ and pure CNTs after the first discharge–charge process at an OCV of 2.1 V. Bottom: The simulated equivalent circuit of the electrode/electrolyte interface for different electrode materials.

As shown in Fig. 7, the Nyquist plots suggests that the semicircle diameter for the TBA-$PMo_{11}V$/CNTs electrode in the high-to-medium-frequency region is smaller compared with the physical mixture of TBA-$PMo_{11}V$ and CNTs, TBA-$PMo_{11}V$, pure CNTs. This result indicates that the TBA-$PMo_{11}V$/CNTs electrode features lower contact and charge-transfer resistance.

Moreover, the equivalent circuit model of the studied system is also presented in Fig. 7 in order to represent the internal resistance of the test battery, in which R_e is the electrolyte resistance, R_{ct} is the charge-transfer resistance, Z_w is the Warburg impedance related to the diffusion of Li^+ ions into the bulk electrode, CPE_{ct} represents the constant-phase element, and C_{int} is a capacitor that represents the accumulation of Li^+ ions in the electrode. It can be seen that for the TBA-$PMo_{11}V$/CNTs electrode, the values of electrolyte resistance (R_e) and charge-transfer resistance (R_{ct}) are 2.03 and 38.04 Ω, respectively, which are lower than those of the physical mixture of TBA-$PMo_{11}V$ and CNTs (3.25 and 62.28 Ω, respectively), TBA-$PMo_{11}V$ (4.57 and 79.56 Ω, respectively) and pure CNTs electrode (3.86 and 102.44 Ω, respectively). This result indicates that the sonication-driven periodic functionalization of TBA-$PMo_{11}V$ onto CNTs not only favours rapid Li^+ ions transport and electrochemical activity during the Li^+ ions insertion/extraction, but also results in the retention of the high electron conductivity of CNTs. As a result, it leads to a significant improvement of the electrochemical performance of the TBA-$PMo_{11}V$/CNTs as anode material for LIBs. In addition, for TBA-$PMo_{11}V$/CNTs electrode, a straight line with a slope of about 45° can be observed at the low frequency, which indicates that the good ionic conductivity of TBA-$PMo_{11}V$/CNTs electrode.[44]

Conclusions

In conclusion, we present the first example of periodically patterned POM/CNT nanocomposites. Control over the amount, size and morphology of crystals deposited is achieved using several experimental parameters. Further, the type of cation and anion deposited can be varied. This will allow the formation of a whole family of electro-active POM/CNT composites where chemical activity and battery performance can be tuned on the molecular level. Initial tests of the POM/CNT composites as anode materials for Lithium ion batteries show significantly improved performance compared with state of the art reference systems and stable discharge capacities of 850 mA h g^{-1} are reported. Future work will expand the use of sonochemistry to deposit electroactive materials on conductive substrates to enable efficient charge transfer across the materials interface.

Acknowledgements

This research was supported by the National Basic Research Program of China (973 program, 2014CB932104), National Science Foundation of China (21222104, U1407127), Fundamental Research Funds for the Central Universities (RC1302, YS1406), China Postdoctoral Science Foundation (2014M560878) and Beijing Engineering Centre for Hierarchical Catalysts. C. S. gratefully acknowledges support by the Deutsche Forschungsgemeinschaft DFG and Ulm University.

Notes and references

1 D. Jariwala, V. K. Sangwan, L. J. Lauhon, T. J. Marks and M. C. Hersam, *Chem. Soc. Rev.*, 2013, **42**, 2824–2860.
2 F. R. Baptista, S. A. Belhout, S. Giordani and S. J. Quinn, *Chem. Soc. Rev.*, 2015, **44**, 4433–4453.
3 C. T. White and T. N. Todorov, *Nature*, 1998, **393**, 240–242.
4 T. Rueckes, K. Kim, E. Joslelevich, G. Y. Tseng, C. L. Cheung and C. M. Lieber, *Science*, 2000, **289**, 94–97.
5 D. Bélanger and J. Pinson, *Chem. Soc. Rev.*, 2011, **40**, 3995–4048.
6 W. Chen, L. Huang, J. Hu, T. Li, F. Jia and Y.-F. Song, *Phys. Chem. Chem. Phys.*, 2014, **16**, 19668–19673.
7 Y. Ji, J. Hu, L. Huang, W. Chen, C. Streb and Y.-F. Song, *Chem. – Eur. J.*, 2015, **21**, 6469–6474.
8 D. Ma, L. Liang, W. Chen, H. Liu and Y.-F. Song, *Adv. Funct. Mater.*, 2013, **23**, 6100–6105.
9 S. Banerjee, T. Hemraj-Benny and S. S. Wong, *Adv. Mater.*, 2005, **17**, 17–29.
10 X. Peng, J. Chen, J. A. Misewich and S. S. Wong, *Chem. Soc. Rev.*, 2009, **38**, 1076–1098.
11 X. Gong, J. Liu, S. Baskaran, R. D. Voise and J. S. Young, *Chem. Mater.*, 2000, **12**, 1049–1052.
12 M. Shim, N. W. Shi Kam, R. J. Chen, Y. Li and H. Dai, *Nano Lett.*, 2002, **2**, 285–288.
13 N. K. Subbaiyan, S. Cambré, A. N. G. Parra-Vasquez, E. H. Hároz, S. K. Doorn and J. G. Duque, *ACS Nano*, 2014, **8**, 1619–1628.
14 C. Y. Li, L. Li, W. Cai, S. L. Kodjie and K. K. Tenneti, *Adv. Mater.*, 2005, **17**, 1198–1202.
15 K. A. Worsley, K. R. Moonoosawmy and P. Kruse, *Nano Lett.*, 2004, **4**, 1541–1546.
16 L. Li, C. Y. Li and C. Ni, *J. Am. Chem. Soc.*, 2006, **128**, 1692–1699.
17 (*a*) Special POM issue: C. L. Hill (guest ed.), *Chem. Rev.*, 1998, **98**, 1–390; (*b*) special POM-themed issue: L. Cronin, A. Müller (guest eds.), *Chem. Soc. Rev.*, 2012, 7325–7648.
18 J. T. Rhule, C. L. Hill, D. A. Judd and R. F. Schinazi, *Chem. Rev.*, 1998, **98**, 327–358.
19 S. Herrmann, M. Kostrzewa, A. Wierschem and C. Streb, *Angew. Chem., Int. Ed.*, 2014, **53**, 13596–13599.
20 S. T. Zheng and G. Y. Yang, *Chem. Soc. Rev.*, 2012, **41**, 7623–7646.
21 S. T. Zheng, J. Zhang, X. X. Li, W. H. Fang and G. Y. Yang, *J. Am. Chem. Soc.*, 2012, **132**, 15102–15103.
22 H. N. Miras, J. Yan, D. L. Long and L. Cronin, *Chem. Soc. Rev.*, 2012, **41**, 7403–7430.
23 D. L. Long, E. Burkholder and L. Cronin, *Chem. Soc. Rev.*, 2007, **36**, 105–121.
24 T. Liu, E. Diemann, H. Li, A. W. M. Dress and A. Müller, *Nature*, 2003, **426**, 59–62.
25 Y.-F. Song, D. L. Long, S. E. Kelly and L. Cronin, *Inorg. Chem.*, 2008, **47**, 9137–9139.
26 J. Zhang, Y.-F. Song, L. Cronin and T. Liu, *J. Am. Chem. Soc.*, 2008, **130**, 14408–14409.
27 Y.-F. Song and R. Tsunashima, *Chem. Soc. Rev.*, 2012, **41**, 7384–7402.
28 S. Omwoma, W. Chen, R. Tsunashima and Y.-F. Song, *Coord. Chem. Rev.*, 2014, **258**, 58–71.
29 C. Busche, L. Vila-Nadal, J. Yan, H. N. Miras, D.-L. Long, V. P. Georgiev, A. Asenov, R. H. Pedersen, N. Gadegaard, M. M. Mirza, D. J. Paul, J. M. Poblet and L. Cronin, *Nature*, 2014, **515**, 545–549.
30 H. Wang, S. Hamanaka, Y. Nishimoto, S. Irle, T. Yokoyama, H. Yoshikawa and K. Awaga, *J. Am. Chem. Soc.*, 2012, **134**, 4918–4924.
31 A. Proust, B. Matt, R. Villanneau, G. Guillemot, P. Gouzerh and G. Izzet, *Chem. Soc. Rev.*, 2012, **41**, 7605–7622.
32 S. Mao, G. Lu and J. Chen, *Nanotechnology*, 2008, **19**, 455610.
33 S. Banerjee and S. S. Wong, *Nano Lett.*, 2002, **2**, 195–200.
34 G. A. Tsigdinos and C. J. Hallada, *Inorg. Chem.*, 1968, **7**, 437–441.
35 C. Sanchez, J. Livage, J. P. Launay and Y. Jeannin, *J. Am. Chem. Soc.*, 1982, **104**, 3194–3202.
36 I. Bar-Nahum, J. Ettedgui, L. Konstantinovski, V. Kogan and R. Neumann, *Inorg. Chem.*, 2007, **46**, 5798–5804.
37 O. K. Park, Y. Cho, S. Lee, H. C. Yoo, H. K. Song and J. Cho, *Energy Environ. Sci.*, 2011, **4**, 1621–1633.
38 K. S. Kim, S. B. Suh, J. C. Kim, B. H. Hong, E. C. Lee, S. Yun, P. Tarakeshwar, J. Y. Lee, Y. Kim, H. Ihm, H. G. Kim, J. W. Lee, J. K. Kim, H. M. Lee, D. Kim, C. Cui, S. J. Youn, H. Y. Chung, H. S. Choi, C.-W. Lee, S. J. Cho, S. Jeong and J.-H. Cho, *J. Am. Chem. Soc.*, 2002, **124**, 14268–14279.
39 D. G. Shchukin, E. Skorb, V. Belova and H. Möhwald, *Adv. Mater.*, 2011, **23**, 1922–1934.
40 (*a*) Y. Ji, L. Huang, J. Hu, C. Streb and Y.-F. Song, *Energy Environ. Sci.*, 2015, **8**, 776–789; (*b*) S. Herrmann, C. Ritchie and C. Streb, *Dalton Trans.*, 2015, **44**, 7092–7104.
41 N. Sonoyama, Y. Suganuma, T. Kume and Z. Quan, *J. Power Sources*, 2011, **196**, 6822–6827.
42 E. Ni, S. Uematsu and N. Sonoyama, *J. Power Sources*, 2014, **267**, 673–681.
43 G. Che, B. B. Lakshmi, E. R. Fisher and C. R. Martin, *Nature*, 1998, **393**, 346–349.
44 L. Huang, J. Hu, Y. Ji, C. Streb and Y.-F. Song, *Chem. – Eur. J.*, 2015, **21**, 18799–18804.